THE JOURNAL OF PHYSICAL CHEMISTRY A

Article

pubs.acs.org/JPCA

Combined Molecular Dynamics, Atoms in Molecules, and IR Studies of the Bulk Monofluoroethanol and Bulk Ethanol To Understand the Role of Organic Fluorine in the Hydrogen Bond Network

Biswajit Biswas, Saptarsi Mondal, and Prashant Chandra Singh*

Department of Spectroscopy, Indian Association for the Cultivation of Science, Kolkata 700032, India

Supporting Information

ABSTRACT: The presence of the fluorocarbon group in fluorinated alcohols makes them an important class of molecules that have diverse applications in the field of separation techniques, synthetic chemistry, polymer industry, and biology. In this paper, we have performed the density function theory calculation along with atom in molecule analysis, molecular dynamics simulation, and IR measurements of bulk monofluoroethanol (MFE) and compared them with the data for bulk ethanol (ETH) to understand the effect of the fluorocarbon group in the structure and the hydrogen bond network of bulk MFE. It has been found that the intramolecular O−H···F hydrogen bond is almost absent in bulk MFE. Molecular dynamics simulation and density function theory calculation along with atom in molecule analysis clearly depict that in the case of bulk MFE, a significant amount of intermolecular O−H···F and C−H···F hydrogen bonds are present along with the intermolecular O−H···O hydrogen bond. The presence of intermolecular O−H···F and C−H···F hydrogen bonds causes the difference in the IR spectrum of bulk MFE as compared to bulk ETH. This study clearly depicts that the organic fluorine (fluorocarbon) of MFE acts as a hydrogen bond acceptor and plays a significant role in the structure and hydrogen bond network of bulk MFE through the formation of weak O−H···F as well C−H···F hydrogen bonds, which may be one of the important reasons behind the unique behavior of the fluoroethanols.

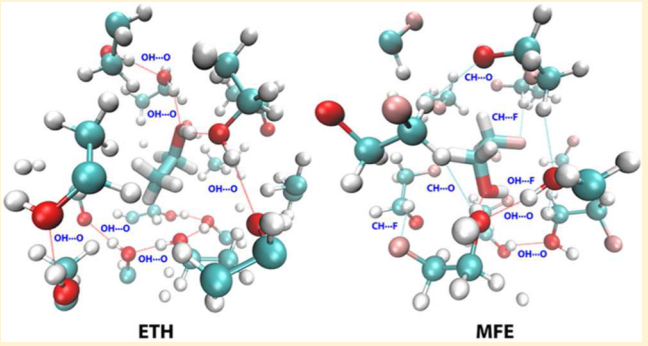

1. INTRODUCTION

Fluorinated alcohols are important class of molecules which have diverse applications in the field of biology and synthetic chemistry.[1−4] Fluorinated alcohols are environmental friendly solvents due to their high melting point and low boiling point in comparison to their nonfluorinated counterparts, which are generally highly polar and solvate water easily. These properties of the fluorinated alcohols make them ideal solvents for the reaction medium, catalysis, and separation. It has been found that the proteins are more stable in the fluorinated alcohol−water mixture than in bulk water as well as being more stable in nonfluorinated alcohol−water mixtures.[5−9] The higher stability of the protein in the aqueous solution of fluorinated alcohols has been assigned to the self-aggregating property of fluorinated alcohols through the weak fluorous interaction.[9,10] Due to the unique properties of the fluorinated alcohols, extensive research attention has been devoted to understand the various physical, chemical, and biological aspects of fluorinated alcohols.

The presence of a fluorocarbon group (C−F) is the main difference between the fluorinated and nonfluorinated alcohols. The C−F group is longer and less polarizable than the C−H group due to the high electronegativity of the fluorine atom. The direction of the dipole moment of the C−F group is opposite to the C−H group and the strength of the C−F bond is higher by 14 kcal/mol, which makes the C−F group more inert and extremely hydrophobic compared to the C−H group.[11,12] Due to the unique physicochemical properties of the C−F group, it tends to self-aggregate, which may cause the different bulk structure and hydrogen bond network of the fluorinated alcohols as compared to the case of nonfluorinated alcohols.

There are several experimental and theoretical studies in which the structure, heterogeneity, and hydrogen bond network of bulk nonfluorinated alcohols as well as their water mixtures have been studied.[13−25] However, the reports on the structure and hydrogen bond network of bulk fluorinated alcohols are sparse.[26−29] The presence of the C−F group increases the acidity of OH group of fluorinated alcohols, making them a strong hydrogen bond donor and simultaneously, a C−F group can also act as a hydrogen bond acceptor.[30−34] Hence, it is interesting to explore the structure and hydrogen bond network of fluorinated alcohols in their bulk medium to understand the involvement of C−F and OH groups. In this paper, we have investigated the structure and hydrogen bond network of bulk

Received: December 21, 2016
Revised: January 16, 2017
Published: January 18, 2017

DOI: 10.1021/acs.jpca.6b12770
J. Phys. Chem. A 2017, 121, 1250−1260

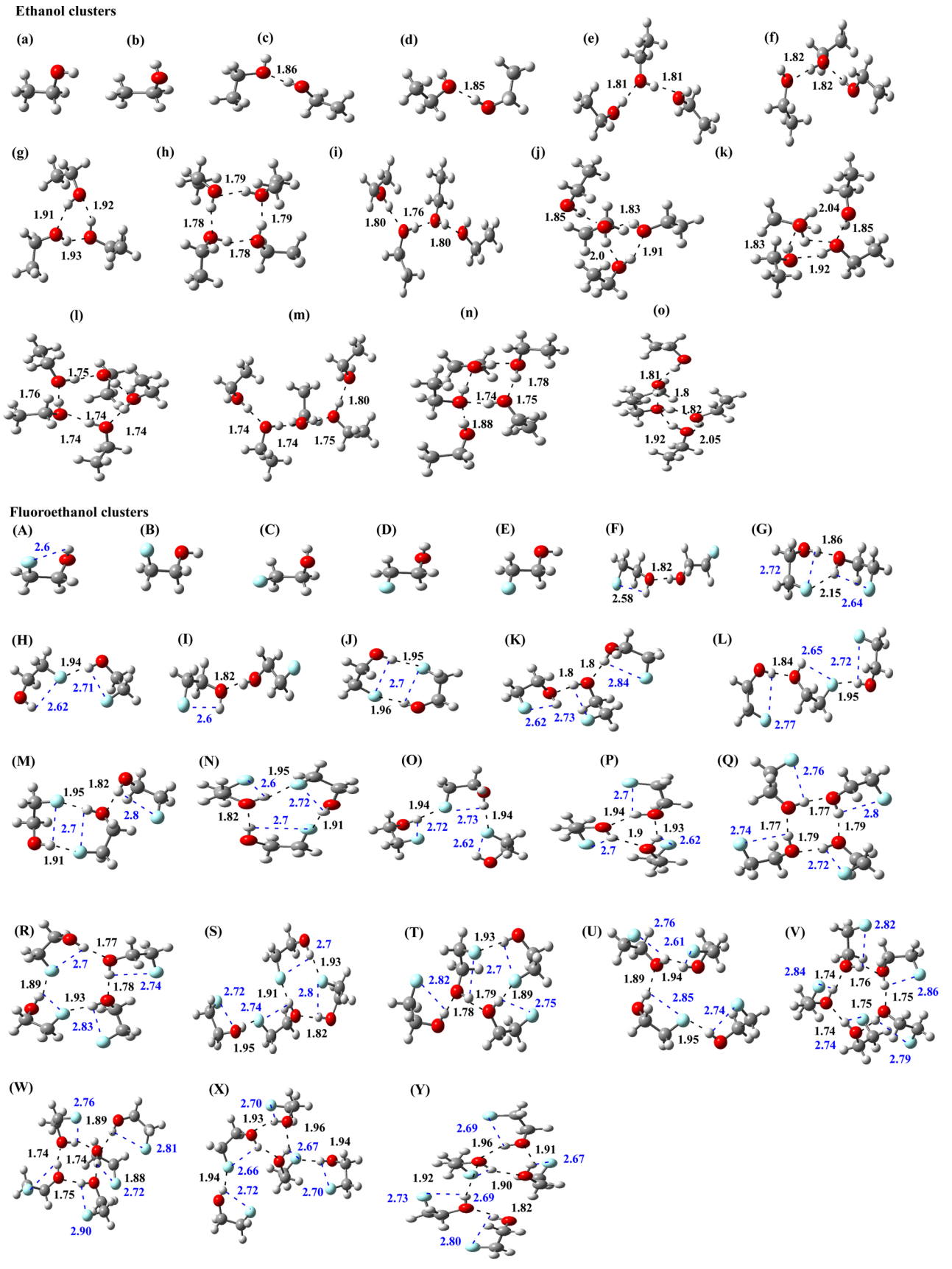

Figure 1. Optimized structures of the ETH and MFE clusters in their respective bulk medium using the B3LYP/6-311++G(d,p) level of theory. The solvent effect has been added using the PCM method. The carbon, hydrogen, oxygen, and fluorine atoms are depicted in ash, white, red and light blue colors, respectively. The unit of intermolecular (black line) and intramolecular (blue line) distances are in Å.

DOI: 10.1021/acs.jpca.6b12770
J. Phys. Chem. A 2017, 121, 1250−1260

monofluoroethanol (MFE) and compared them with those of bulk ethanol (ETH) using the molecular dynamics (MD) simulation, density function theory calculation, atoms in molecule (AIM) analysis, and experimental IR studies. MFE was chosen as we are interested in understanding the role of a single fluorine in the structure and hydrogen bond network of alcohols in their bulk medium. This study clearly depicts that C−F group of MFE acts as a hydrogen bond acceptor and plays a significant role in the structure and hydrogen bond network of bulk MFE through the formation of weak intermolecular O−H···F and C−H···F hydrogen bonds.

2. METHODS

The infrared spectra of alcohols have been measured by the Fourier transform infrared spectrometer (Nicolet iS10, Thermo fisher) operating in the attenuated total reflection mode (ATR). The FTIR spectrometer is equipped with a deuterated triglycine sulfate (DTGS) detector. The ATR crystal (PIKE, GladiATR) is made of a monolithic diamond crystal with an incident angle of 45°. The resolution of the IR measurement was 2 cm^{-1}. The ATR correction has been performed for the measured IR spectra. N_2 gas was flowed throughout the measurement to remove the effect of atmospheric vapors. The IR spectra of different samples have been measured in the water bending region to make sure that samples have no contamination of water or moisture as shown in the Supporting Information (Figure S1). All the measurements have been performed at room temperature (25 ± 3 °C).

The different types of clusters of ETH and MFE up to pentamer size have been optimized in their bulk medium using the B3LYP method with the 6-311++G(d,p) basis set. The optimization has been performed using the polarizable continuum model (PCM) to incorporate the effect of solvents. Frequency calculation has been performed for all the structures in their bulk medium to confirm the nature of optimized structures. We have performed the anharmonic calculation in their bulk medium to get the reliable scaling factors for the different mode of alcohols. The frequencies were found to be real for all the structures, confirming that the particular structure is a minimum energy structure. All the calculations have been performed with frozen core approximation, and optimization has been done with standard convergence criteria. Further, stabilization (ΔE_{st}) and incremental association (ΔE_{in}) energies have been calculated to understand the energetics of different size of the clusters of alcohols. The energy difference between the complex and monomer provides the stabilization energy whereas the incremental association energy depicts the energy difference between the two consecutive sizes of clusters. The energies have been corrected for the basis set superposition error (BSSE) using the counterpoise method. We have also calculated the weighted average energies and IR spectrum. The weight for each cluster has been obtained from the relative population calculation, which has been estimated from the Gibbs free energies of the respective clusters. All the calculations have been performed by using the G09 suites of program.[35] The nature of bonding between different alcohol molecules has been investigated by AIM calculation.[36]

MD simulations of ETH and MFE were carried out using the all-atom simulation method incorporated in GROMACS molecular dynamics simulation package.[37] The all-atom (OPLS-AA) parameters for ETH were used as available in GROMACS topology whereas the topology of MFE was constructed using automated topology builder software (ATB)[38] by attaining the correct density of MFE via tuning of its partial charges. Each simulation box has ∼2500 alcohol molecules. Each trajectory was first equilibrated in a *NVT* ensemble for 500 ps at 800 K to remove the biased structural dependence followed by the *NPT* ensemble for 1 ns at 300 K and 1 bar pressure after steepest descent energy minimization of 5000 steps. Subsequently, the equilibrated configuration was subjected to a production run of another 5 ns in the *NPT* ensemble at 300 K and 1 bar pressure. The temperature was kept constant using the Berendsen thermostat[39] with a time constant (τ) of 0.5 ps^{-1}, and the pressure of the system was kept constant by using the Parinello−Rahman barostat[40] with a τ of 1.0 ps^{-1}. Each simulation used a time-step of 2 fs with periodic boundary conditions. Nonbonded force calculation with a grid was employed for neighbor searching. Neighbor list generation was performed after every 10 steps. A cutoff radius of 1.2 nm was used for both neighbor list and van der Waal's interaction.

3. RESULTS AND DISCUSSION

a. Structure and Energetics. Water molecules can form an extended hydrogen-bonded network by using two lone pairs of oxygen as well as two hydrogen atoms. However, unlike water, alcohols have only two lone pair and one hydrogen atom due to which they prefer to aggregates in the form of clusters of different size. Hence, to get insight into the structural information about the ETH and MFE in their respective bulk mediums, we have optimized the structures of different type of ETH and MFE clusters containing the maximum of five molecules using the PCM method at B3LYP/6-311++G(d,p) level of theory. The optimization has been done up to the five alcohol molecules as the earlier MD simulations suggests that the biggest cyclic structure of bulk ETH contains five molecules.[25] Figure 1 depicts the optimized structures of the different size of ETH and MFE clusters along with their inter- and intramolecular hydrogen bond distances. The relative population and energetics of different clusters of ETH and MFE have been depicted in Table S1. The monomer of ETH in bulk ETH solution exists in two different conformations gauche and anti as shown in Figure 1a,b. The dimer of ETH forms donor (D)−acceptor (A) type hydrogen-bonded species (Figure 1c,d). The most populated and most stable structure of the ETH trimer is DDA type of linear chain structure (Figure 1e) as compared to the closed ring structure (Figure 1g) whereas closed-ring structure is the most stable and populated structure for the tetramer and pentamer clusters (Figure 1h,l). This is in accordance with the earlier MD simulations in which it has been found that the small size of ETH clusters preferred to form the linear chain structure.[14,25]

Five different conformers of MFE having gauche (Figure 1A−C) or trans (Figure 1D,E) forms with respect to the F−C−C−O moiety have been found to be stable in their bulk medium. The gauche conformer of MFE is the most stable with the total relative population of 95% in bulk MFE. The most stable structure of the gauche form (A) has the O−H group directed toward the fluorine atom of the MFE at a distance of 2.6 Å, indicating the possibility of intramolecular O−H···F interaction and enforcing the enhanced gauche effect. The other two gauche forms (B, C) have a lower probability of the intramolecular O−H···F hydrogen bond, resulting in the lower population. The trans form of the MFE has a very low population (D and E, ∼0.05%). The most populated structure for the dimer of MFE (F, ∼50%) has the D−A kind of

DOI: 10.1021/acs.jpca.6b12770
J. Phys. Chem. A 2017, 121, 1250−1260

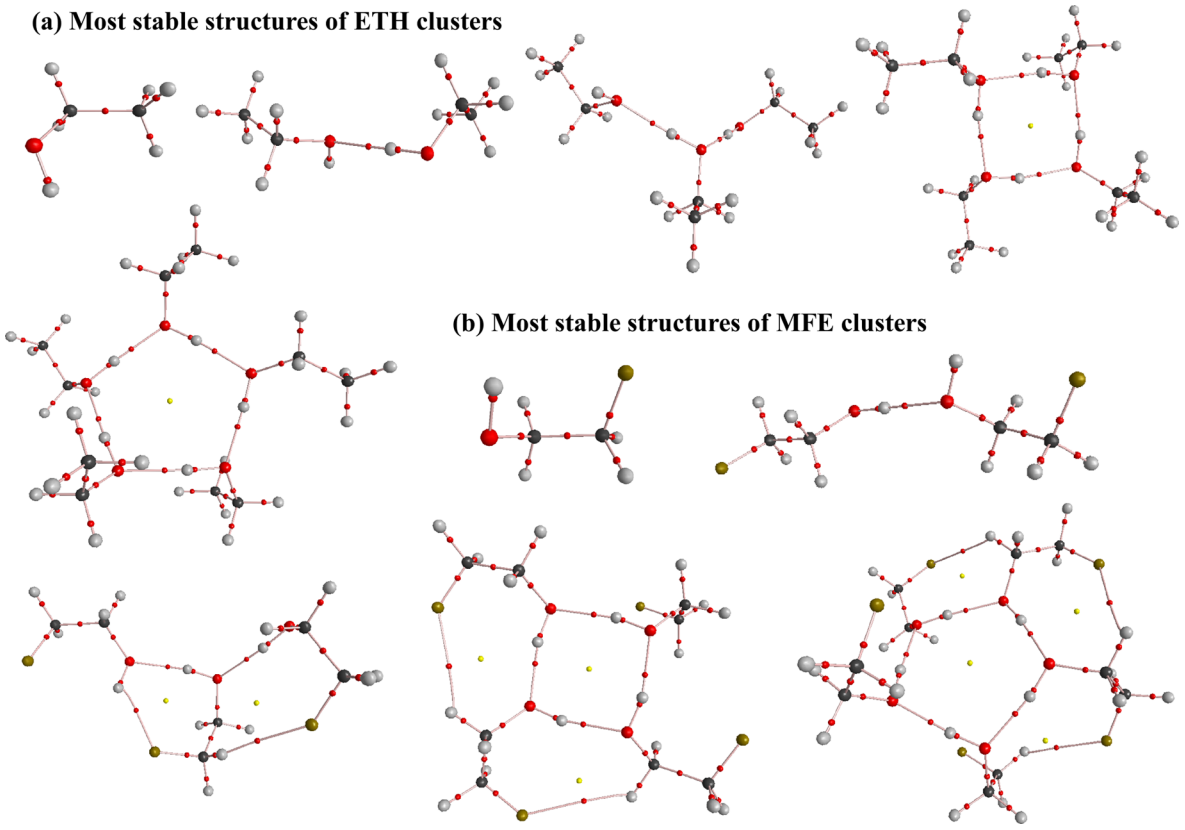

Figure 2. Molecular graph of topology of the electron density for the most stable structures of ETH and MFE clusters in their respective bulk medium calculated at the B3LYP/6-311++G(d,p) level of theory.

intermolecular O−H···O hydrogen bond structure, similar to the structure of the dimer of ETH. G and H are other two most populated structures for the dimer of MFE in which G has O−H···O and O−H···F interactions and H has O−H···F interaction between interacting MFEs. The relative population of the closed-ring type of DADA structure (J) of the MFE dimer is extremely lower than the population of the D−A type of linear hydrogen-bonded complexes (F, G, H). The most populated structure of MFE trimer (K, 75% population) has the O−H···O type of DDA linear hydrogen-bonded structure. Other structures of MFE trimer contain mainly the O−H···F interaction, and their population is relatively small. The most populated tetramer and pentamer clusters of MFE is the closed-ring type of structure consisting of the O−H···O hydrogen bond (Q and V, population is 98%). Interestingly, the population ofthe O−H···F hydrogen-bonded structure for a higher order of clusters containing more than three MFE is very low. One interesting observation is that the intramolecular O−H···F distance within a MFE increases with the increases of the number of MFE molecules in the cluster, indicating that the intermolecular O−H···O and O−H···F interactions weakens the intramolecular O−H···F interaction. The main structural difference between ETH and MFE appears primarily for the small size of clusters of MFE where the population of O−H···F interacting clusters is significant; hence, the total population of the O−H···O hydrogen-bonded clusters for MFE is lower than that for ETH.

Further, we have performed the AIM analysis on all the structures of ETH and MFE to get insight in to the different kind of interaction of ETH and MFE clusters in their bulk mediums. Figures 2a,b and S2 show the molecular graph of the electron density for the structures of different size of ETH and MFE clusters. The values of topological parameters such as electron density (ρ), Laplacian (∇^2), total electronic energy density (H), and its component local electronic kinetic energy density (G), local potential energy density (V) at BCP are shown in the Table S2. A (3, −1) bond critical point (BCP) with a positive Laplacian (∇^2) indicates the presence of noncovalent interaction, whereas, the presence of a (3, + 1) ring critical point (RCP) shows that the corresponding structure is cyclic in nature. The values of topological parameters shown in Table S2 are in the range of acceptable values for the noncovalent interaction.[41−44] It can be clearly seen that the linear structures of alcohols have the (3, −1) BCP between the O−H···O intermolecular hydrogen bond whereas (3, +1) RCP is present along with (3, −1) BCP for the closed structure assert their cyclic nature. The hydrogen-bonded complexes of MFE shows the presence of (3, −1) BCP for the intermolecular O−H···O and O−H···F interactions confirming the presence of these hydrogen bonds in the linear MFE complexes. The values of topological parameters for the intermolecular O−H···F hydrogen bond are lower than those of the O−H···O hydrogen bond, indicating that the strength of intermolecular O−H···F hydrogen bond is weaker than that of O−H···O in bulk MFE. Other noticeable observation for trimer and higher size of MFE clusters is the presence of a (3, −1) BCP for the C−H···F contact between the C−H group of CH_2F of one MFE with the F−(CH_2) of another MFE indicating the existence of weak intermolecular C−H···F hydrogen bond interaction in bulk MFE. One most interesting observation is the absence of (3, −1) BCP for the intramolecular O−H···F hydrogen bond in MFE monomer as

DOI: 10.1021/acs.jpca.6b12770
J. Phys. Chem. A 2017, 121, 1250−1260

well as their clusters, indicating the extremely weak or the almost absence of intramolecular O−H···F hydrogen bond in their bulk medium. Indeed, the lack of intramolecular O−H···F hydrogen bond for the MFE monomer has been pointed out in the earlier studies of MFE in the gas phase as well as nonpolar medium.[27,45] The AIM study on the MFE clusters clearly depict that the intermolecular O−H···O, O−H···F along with weak C−H···F hydrogen bond stabilizes bulk MFE and the role of intramolecular O−H···F hydrogen bond is not significant.

Table 1 shows the stabilization energy (ΔE_{st}) and incremental association energy (ΔE_{in}) along with their weighted average values (ΔE_{wst}, ΔE_{win}) for the different size of the clusters of ETH and MFE. The stabilization energy for the ETH and MFE increases with the increase of their cluster size. The incremental association energies for the tetramer and pentamer clusters of ETH and MFE are higher than that of the trimer structure, which could be due to the fact that the tetramer and pentamer clusters of ETH and MFE are forming closed cyclic structures whereas the most stable structure of the trimer is a linear structure. BSSE correction of the energetics for the different size of clusters for ETH and MFE does not change the order of the energetics except that it decreases the absolute values.

Table 1. Stabilization (E_{st}) and Incremental Association (ΔE_{in}) Energy (kJ/mol) for the Most Stable Structures of the ETH and MFE in Their Respective Bulk Mediums Calculated at the B3LYP/6-311++G(d,p) Level of Theory[a]

structure	ΔE_{st}	ΔE_{wst}	ΔE_{in}	ΔE_{win}
		ETH		
dimer	4.3 (3.0)	4.2 (3.3)	4.3 (3.0)	4.3 (3.0)
trimer	9.2 (6.9)	9.2 (6.8)	4.9 (3.7)	4.9 (3.7)
tetramer	18.6 (14.4)	18.1 (14.0)	9.3 (7.5)	8.9 (7.1)
pentamer	25.1 (19.7)	23.5 (18.3)	6.5 (5.3)	4.8 (3.8)
		MFE		
dimer	2.6 (1.6)	3.0 (2.0)	2.6 (1.6)	3.0 (2.0)
trimer	9.7 (7.4)	8.9 (6.8)	4.9 (3.9)	4.2 (3.3)
tetramer	18.4 (14.6)	18.3 (14.5)	8.8(7.2)	8.6 (7.1)
pentamer	24.8 (20.0)	24.7 (19.9)	6.4 (5.4)	6.3 (5.4)

[a]The BSSE corrected energies are provided in parentheses. Weighted average energies (kJ/mol) for each size of clusters are also calculated.

We have performed the MD simulation of bulk ETH and MFE (Figure 3a,b) to ensure the results about the hydrogen bond network of ETH and MFE obtained from the density function calculations. The snapshots of the MD simulation of bulk ETH show (Figure 3a) the presence of an intermolecular O−H···O hydrogen bond in their hydrogen bond network whereas for the case of MFE (Figure 3b), a significant amount of O−H···F, C−H···F, and C−H···O interactions are present along with intermolecular O−H···O hydrogen bond. Figure 3c shows the radial distribution $g(r)$ for the $H_{(OH)}$ and $O_{(OH)}$ of ETH (black line) and shows a sharp peak at the 2.0 Å depicting the intermolecular O−H···O hydrogen bond between the ETH molecules. The observed peak position of the $g(r)$ for ETH is in the line with the earlier simulation results.[14,19,23−25,46] The first peak of the $g(r)$ for the $H_{(OH)}$ and $O_{(OH)}$ of MFE (Figure 3c, red line) is slightly shifted (1.8 Å), and the intensity of the peak is lower than that of ETH. The $g(r)$ for the MFE shows that the number of intermolecular O−H···O hydrogen bonds in MFE is lower than that in ETH although the distance for the intermolecular O−H···O hydrogen bond is smaller in MFE. The $g(r)$ for the $H_{(OH)}$ and $F_{(CH_2F)}$ of MFE shows a broad peak centered at 2.5 Å (Figure 3c, blue line), which shows that the O−H···F interaction exists in the MFE. MD simulation clearly depicts that weak intermolecular O−H···F hydrogen bond along with the strong intermolecular O−H···O hydrogen bond exists in the case of MFE, which is in the line with the results from the DFT calculation as well as AIM analysis discussed earlier. Further, we have also calculated the $g(r)$ around the terminal CH group of ETH (CH_3) and MFE (CH_2F) to understand the hydrogen bond network around the terminal CH group of ETH as well as MFE and the results are shown in Figure 3d. For the ETH case, the intensity of the peak for the $g(r)$ between the CH_3 and O of ETH within 3.0 Å is extremely weak, indicating that the statistical probability of the intermolecular interaction between the terminals CH_3 and oxygen of ETH in their bulk medium is sparse. However, the $g(r)$ between the $CH_{(CH_2F)}$ and $O_{(OH)}$ as well as $F_{(CH_2F)}$ of MFE shows a comparatively intense shoulder ∼2.7 Å, which shows that weak intermolecular C−H···O and C−H···F interactions exist in bulk MFE. Interestingly, the intensity of the first peak of the $g(r)$ for the CH···F interaction is higher than that for the C−H···O interaction, indicating that the probability of C−H···F interaction is higher than that for the C−H···O in bulk MFE. Indeed, the AIM calculation also shows the existence of the CH···F interaction in MFE, which is in line with the MD simulation results. In summary, the MD simulation and AIM along with the density function theory calculations clearly show that the C−F group of MFE plays an important role in the hydrogen bond network of the MFE through the weak O−H···F, CH···F, and CH···O interactions.

b. Vibrational Frequency. Infrared spectroscopy is a sensitive tool to understand the hydrogen bond network of the bulk medium. Hence, to get the insight feature of the hydrogen bond network of bulk ETH and MFE, we have measured the IR spectra of bulk ETH and MFE in the OH and C−H stretching regions covering the range 2800−3800 cm^{-1}. Figure 4a shows the normalized IR spectra of the ETH (black line) and MFE (red line) in the OH stretching region. It is clearly evident that the IR spectrum of MFE is slightly broad and blue-shifted compared to the ETH spectrum. Apart from that, the IR spectrum of MFE shows additional broad feature in the region 3550−3650 cm^{-1} with the peak at the 3580 cm^{-1}. The blue shift feature and the additional peak feature of the IR spectrum of MFE is clearly evident in the difference spectrum shown in the inset of the Figure 4a. The relatively blue-shifted IR spectrum of MFE shows that the average hydrogen bond strength of MFE is weaker than that of ETH whereas the broad spectrum of MFE shows that hydrogen bond environment of MFE is more inhomogeneous than that of ETH. The presence of additional peak in the high-frequency region of the OH stretching of MFE indicates the presence of a weak hydrogen bond environment. The normalized IR spectrum of ETH (Figure 4b, black line) in the C−H stretching region shows four bands at 2880, 2898, 2926, and 2972 cm^{-1}. The vibrational feature for bulk MFE (Figure 4b, red line) in the C−H stretching region is also different from the ETH. The peak feature in the region 2850−2900 cm^{-1} for MFE is clearly well resolved compared to the broad feature for ETH in the same region. Moreover, the peak around the 2950 cm^{-1} is broad and shows the double-peak feature centered at the 2960 and 2985 cm^{-1}. The different IR data for ETH and MFE clearly indicate

DOI: 10.1021/acs.jpca.6b12770
J. Phys. Chem. A 2017, 121, 1250−1260

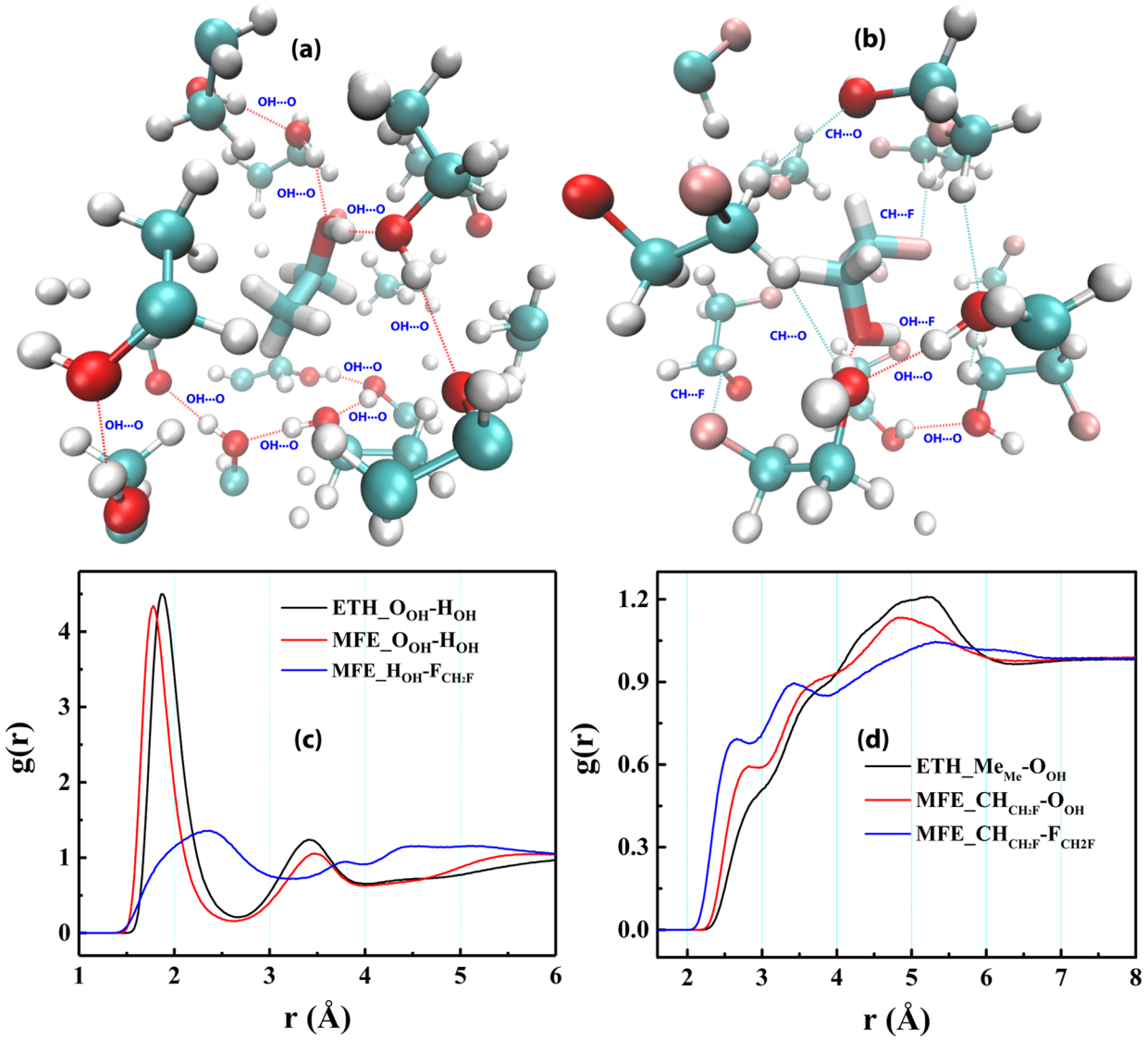

Figure 3. Snapshot of the structure and the hydrogen bond network of ETH (a) and MFE (b) in their respective bulk mediums obtained from the MD simulation. $g(r)$ between the $H_{(OH)}$ and $O_{(OH)}$ of ETH (c, black) and of MFE (c, red) along with $g(r)$ between the $H_{(OH)}$ and $F_{(CH_2F)}$ of MFE(c, blue). $g(r)$ between the CH_3 and oxygen of ETH (d, black) and between the CH_2F and oxygen (d, red) as well as fluorine (d, blue) of MFE, respectively.

that the C−F group of MFE plays a significant role in the restructuring of the hydrogen-bonding network.

To understand the role of C−F in the restructuring of the hydrogen bond network of MFE, we have calculated the IR spectra of each size of clusters of ETH and MFE (Figure S3) along with their weighed average IR spectra in the O−H and CH stretching regions (Figure 5). The calculated IR spectra for the monomers of ETH in their OH stretching region shows a feature around ∼3630 cm^{-1}; however, the experimental IR spectrum of the ETH does not have any feature around ∼3630 cm^{-1} depicting that ETH does not exist in the monomer form in their bulk medium. In fact, several simulation studies have shown that ETH does not exist in monomer form in their bulk medium and form the higher order of clusters.[14,24,25] With the increase of the cluster size, the vibrational band positions of the hydrogen-bonded OH of ETH clusters are red-shifted compared to the bands of the free OH of ETH. On comparison of the experimental IR data of ETH with the weighted average IR spectra of the different size of ETH clusters, it appears that the population of the pentamer size of clusters is lower than that of the dimer, trimer, and tetramer in their bulk medium, which is in line with the prediction of the earlier simulation studies.[14,25]

From the AIM analysis and MD simulation, it is apparent that MFE forms O−H···O and O−H···F hydrogen bonds in their bulk medium as compared to the presence of only the O−H···O hydrogen bond in bulk ETH. MFE in their bulk medium mainly exists in the gauche form (∼95% population) and the calculated OH stretching of MFE appears ∼3620 cm^{-1}. The vibrational frequency of the gauche monomer is slightly lower than the frequencey of the trans structure, which could be due to the extremely weak intramolecular O−H···F hydrogen bond. The calculated vibrational feature for the O−H···O hydrogen-bonded dimer of MFE appears ∼3400 cm^{-1} (structure F, Figure S3) whereas the O−H···F hydrogen bond appears in the high-frequency region around ∼3590 cm^{-1} (structure G, Figure S3). The calculated weighted average IR spectrum of the dimer of the MFE also shows the peak at the high-frequency region

DOI: 10.1021/acs.jpca.6b12770
J. Phys. Chem. A 2017, 121, 1250−1260

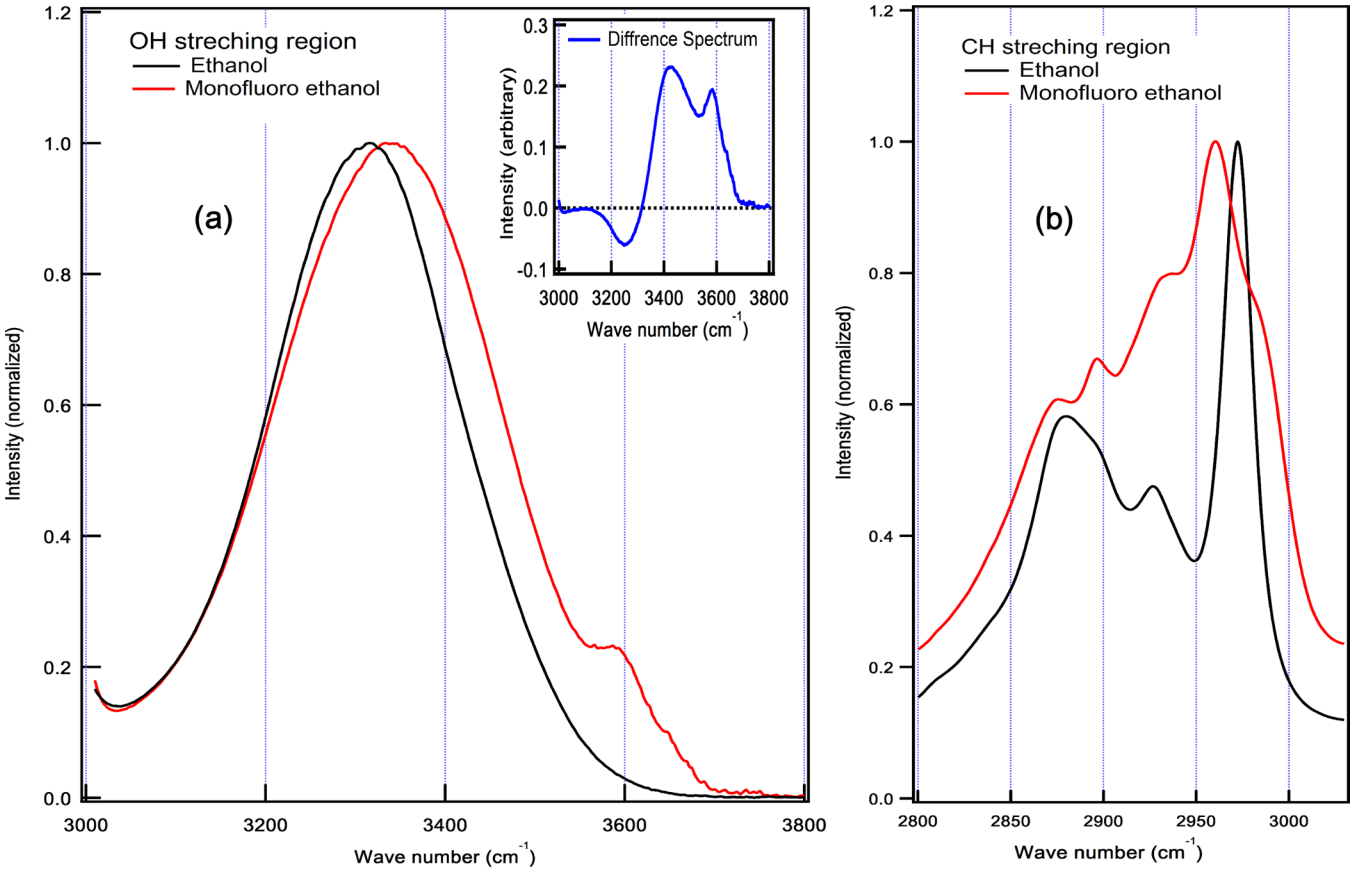

Figure 4. Normalized IR spectra of ETH and MFE in the OH (a) and C−H (b) stretching regions. The difference spectrum between ETH and MFE in the OH stretching regions are shown in the inset of (a).

around ∼3590 cm^{-1} (O−H···F hydrogen bond) apart from the peak at 3400 cm^{-1} (O−H···O hydrogen bond). Similarly, the calculated weighted average spectra of the trimer and tetramer clusters of MFE in the bulk medium shows the intense peak in the low-frequency regions (3250−3400 cm^{-1}) along with a weak intense peak in the high-frequency regions (3560−3580 cm^{-1}). For the pentamer clusters of MFE, there is almost no intensity in the high-frequency region of weighted average IR spectrum as the main contributor is the structure V (98%), which is the cyclic structure having only a O−H···O hydrogen bond. It is important to note that the vibrational feature for the intermolecular O−H···F hydrogen-bonded (∼3550−3610 cm^{-1}) system appears to be slightly red-shifted compared to the position of the free OH of MFE (∼3650 cm^{-1}) or intramolecular O−H···F hydrogen-bonded clusters (∼3630 cm^{-1}). On the basis of the calculation, we assign the vibrational band of MFE in the region 3000−3580 cm^{-1} to the O−H···O hydrogen-bonded part of MFE clusters. The broad spectral feature in the high-frequency region ∼3550−3610 cm^{-1} has been assigned to the weak intermolecular O−H···F hydrogen-bonded part of MFE, which is mainly coming from the dimer or trimer size of clusters of bulk MFE.

Interestingly, the fluorine substitution makes the OH group of MFE more acidic than the OH of ETH; hence, it should form a stronger hydrogen bond. However, the experimental IR data show that the average strength of the OH hydrogen bond of MFE is weaker than that for the bond in ETH. In the case of MFE, a significant amount of weak intermolecular O−H···F hydrogen bonding is taking place at the cost of strong intermolecular O−H···O hydrogen bonding as compared to the presence of only a strong intermolecular O−H···O hydrogen bond in the case of ETH. Hence, the average hydrogen bond strength in the case of MFE is weaker than that for ETH. The presence of a different type of hydrogen bond environment in the case of MFE (O−H···O and O−H···F) makes the spectral width broader than that for ETH.

The calculated weighted average IR spectra of the different size of clusters show the spectral features ∼2860, 2875, 2920, and 2950 cm^{-1} in the C−H stretching region. The calculated IR spectra of ETH in the C−H stretching region (Figure 5c) are slightly red-shifted compared to the experimental data, which show that the scaling factor used for the different modes of C−H stretching frequency is not sufficient. We have also calculated the CH_3 and CH_2 bending modes of the different size of clusters of ETH (Table S3) and the distribution of the stretching and bending mode of the CH_3 and CH_2 are shown in Figure 6a,b. The calculated frequency distribution data in the C−H region of ETH (Figure 6a,b) show that the CH_3 symmetric stretching of the different size of ETH clusters has the overlapping region with the CH_2 symmetric stretching in the ∼2860 cm^{-1} region, which is close to the observed experimental feature at 2880 and 2898 cm^{-1}. Frequency distribution data also show that the center of the CH_3 asymmetric stretching (∼2945 cm^{-1}) overlaps with the center position of the two quanta of the CH_2 bend (∼1470 cm^{-1}). Similarly, the center of the CH_2 asymmetric stretching (∼2900 cm^{-1}) has a weak overlap with the two quanta of the CH_3 bend (∼1436 cm^{-1}). The calculated frequency data show that there may be a possibility of Fermi resonance between the CH_3 asymmetric stretching with the CH_2 bend and CH_2 asymmetric

DOI: 10.1021/acs.jpca.6b12770
J. Phys. Chem. A 2017, 121, 1250−1260

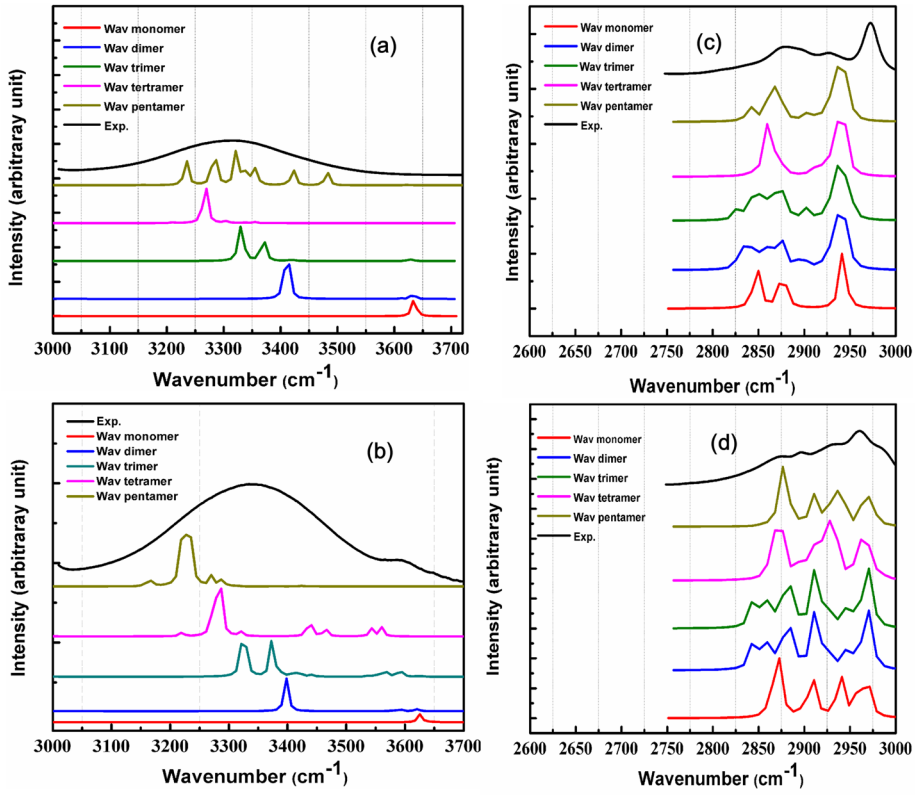

Figure 5. Calculated weighted average IR spectra of the different size of clusters of ETH and MFE in the OH (a, b) and CH (c, d) stretching regions, respectively. The black line in each panel shows the experimental IR spectra of ETH and MFE in the OH and C−H stretching regions. The calculation has been performed at the B3LYP/6-311++G(d,p) level of theory. PCM model has been used to incorporate the effect of solvent.

stretching with the CH_3 bend. Hence, the peak observed at 2926 cm^{-1} may have the contribution from the CH_2 asymmetric stretching as well as the Fermi resonance contribution from CH_3 bending and the peak observed at the 2972 cm^{-1} is probably due to the CH_3 asymmetric stretching along with the Fermi resonance contribution from CH_2 bend. Indeed, the vibrational feature of the ETH in the C−H stretching region has been studied by various different experimental methods. On the basis of earlier experimental studies, the band features at 2880 and 2898 cm^{-1} were assigned to the overlapping symmetric stretching modes, the band feature at 2926 cm^{-1} was assigned to the CH_3 Fermi resonance modes and the antisymmetric modes, and the band at the 2972 cm^{-1} was assigned to the CH_3 antisymmetric stretching and CH_3 Fermi resonance modes.[13] The theoretically calculated IR data for the C−H stretching of ETH in this study are in qualitatively good agreement with the earlier assignments obtained from the polarized Raman experiments.[13,20]

The calculated weighted average spectra and frequency distribution data for the different size of MFE clusters show that the symmetric CH stretch of the CH_2 group is around ∼2875 cm^{-1} whereas the center position of the symmetric CH stretch of the FCH_2 is around ∼2910 cm^{-1} (Figure 6c,d). The calculation data show that the peak position symmetric CH stretch of the FCH_2 and CH_2 groups of MFE is more separated than the symmetric CH stretch of the CH_3 and CH_2 groups of ETH. Hence, the peak position observed at the 2874 and 2896 cm^{-1} in the experimental data has been assigned to the CH stretch of the CH_2 group and FCH_2 of MFE, respectively. The experimentally observed peak position at the 2928 cm^{-1} matches with the asymmetric stretching of the CH_2 group of MFE (∼2930 cm^{-1}). The two quanta of the bending mode of the FCH_2 group of MFE (∼1460 cm^{-1}) matches with the asymmetric stretching of the CH_2 group of MFE; hence, there is the possibility of Fermi resonance. We tentatively assign the experimentally observed band at 2928 cm^{-1} to the asymmetric stretching of the CH_2 group of MFE as well as to the Fermi resonance arising from the bending mode of the FCH_2 group of MFE. The experimentally observed broad and double-peak feature centered at 2960 and 2985 cm^{-1} could be either due to the Fermi resonance caused by the CH_2 bending mode or due to the asymmetric C−H stretching mode of the FCH_2 group of MFE, which is involved in a different kind of hydrogen bond environments. The calculated frequency distribution data for the CH_2 bending mode are centered around ∼1430 cm^{-1} whereas the asymmetric stretching mode of FCH_2 group of MFE is centered around ∼2975 cm^{-1}. Hence, the two quanta of the CH_2 bending mode cannot be involved in the Fermi resonance with the asymmetric stretching mode of the FCH_2 group as observed in the case of ETH. On the basis of the calculation data, we assign the double-peak feature centered at 2960 and 2985 cm^{-1} to the asymmetric C−H stretching mode of the FCH_2 group of MFE, which is involved in different kinds of hydrogen-bonding environments. Indeed, the C−H group of the FCH_2 of MFE is more acidic than the CH group of CH_3 of ETH due to the electron with drawing nature of the fluorine molecule. Due to the increased acidity of the C−H group of the FCH_2, it can form intermolecular hydrogen bonds with the fluorine and oxygen atom of another MFE via C−H···F and C−H···O interactions. Earlier AIM and molecular dynamics simulation have shown the presence of C−H···F and C−H···O hydrogen bonds in bulk MFE. From the frequency

DOI: 10.1021/acs.jpca.6b12770
J. Phys. Chem. A 2017, 121, 1250−1260

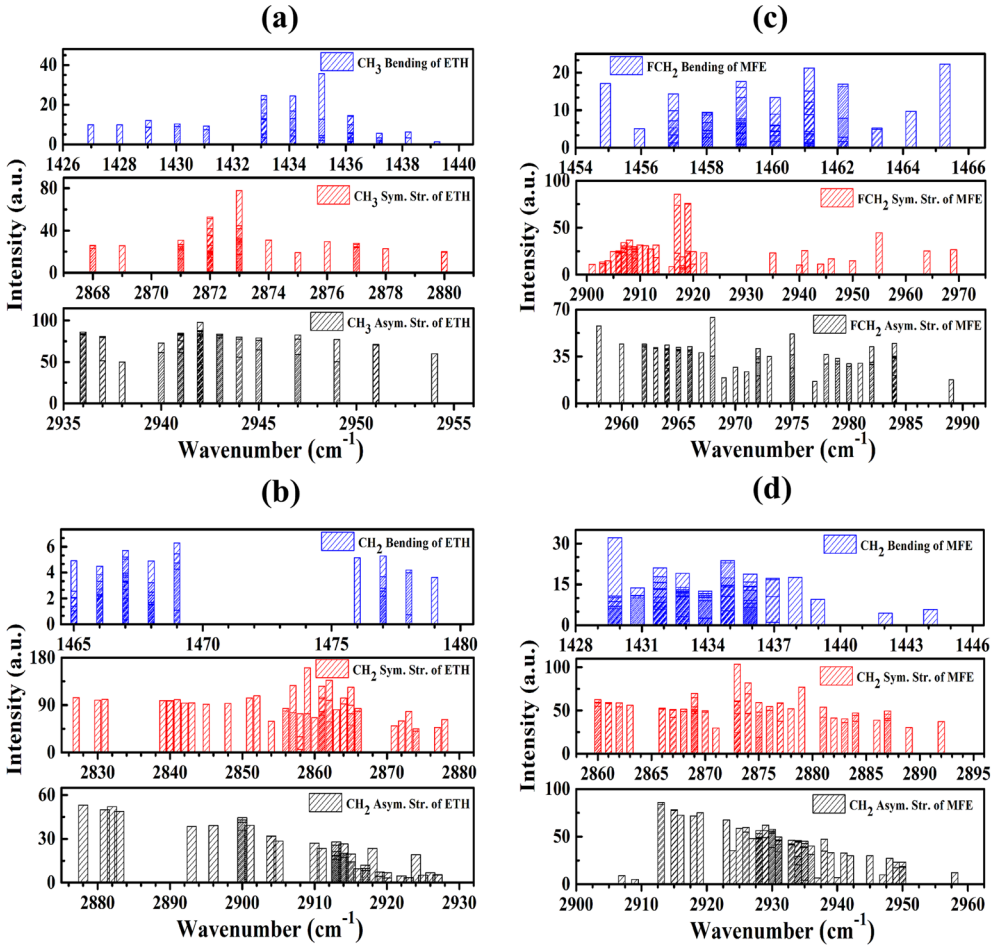

Figure 6. Calculated frequency distribution data for symmetric, asymmetric C−H stretching and bending modes of the different size of clusters of ETH (a, b) and MFE (c, d) in their bulk medium calculated at the B3LYP/6-311++G(d,p) level of calculation. The PCM model has been used to incorporate the effect of solvent.

calculation data, we have observed that the asymmetric C−H stretching mode of the CH_2F group of different sizes of clusters of MFE gets slightly blue-shifted when it has the C−H···F interaction (structure K, N, O, U, V) as compared to the case of other free C−H groups of the same clusters. In the literature also it has been shown that C−H stretching gets blue-shifted when it forms the C−H···F hydrogen bond whereas C−H···O hydrogen-bonded systems are red-shifted.[47,48] On the basis of this observation, we assign the band observed at 2960 cm^{-1} to the asymmetric C−H stretching mode of CH_2F group which is free or C−H···O hydrogen bonded whereas the shoulder at the 2985 cm^{-1} has been assigned to the asymmetric C−H stretching mode of the CH_2F group that forms the weak C−H···F interaction with another MFE molecule in their bulk medium.

4. CONCLUSION

IR measurements along with the DFT, AIM, and MD simulations have been performed on bulk ETH and MFE to understand the role of the fluorocarbon group in the structure and the hydrogen bond network of bulk MFE. The IR spectrum of MFE in the OH stretching region is blue-shifted and broad with an additional feature in the high-frequency region of the OH stretching as compared to case for ETH. The presence of the peak in the high-frequency region of the OH of MFE indicates the presence of weakly hydrogen-bonded species in MFE as compared to the case for ETH. MD simulation, density function calculations, and the AIM analysis indicate that a significant amount of weak intermolecular O−H···F hydrogen bond is present along with the O−H···O hydrogen bond in bulk MFE. In the case of MFE, a significant amount of weak intermolecular O−H···F hydrogen bond forms at the cost of a strong intermolecular O−H···O hydrogen bond as compared to the presence of only a strong intermolecular O−H···O hydrogen bond in the case of ETH. Hence, the average hydrogen bond strength in the case of bulk MFE is weaker than that of ETH. The presence of different types of hydrogen bond environments in the case of bulk MFE (O−H···O and O−H···F) makes the spectral width broader than that of bulk ETH. The IR spectrum of bulk MFE in the C−H stretching region is different from that of ETH and shows a double-peak feature in the CH stretching region 2950−3000 cm^{-1} in comparison to the single peak in the case of ETH. The double-peak feature in the C−H stretching region of MFE has been assigned to those CH_2F groups of MFE that form the C−H···O and C−H···F hydrogen bonds in their bulk medium. In the literature it has been described that the hydrogen bond accepting capability of the organic fluorine is very poor; however, it is clearly evident from this study that the fluorocarbon group of MFE is not inert and acts as a hydrogen bond acceptor through the formation of the weak O−H···F and

DOI: 10.1021/acs.jpca.6b12770
J. Phys. Chem. A 2017, 121, 1250−1260

C−H···F hydrogen bonds, which may be one of the important reasons behind the unique behavior of the fluoro-ETHs.

■ ASSOCIATED CONTENT

Supporting Information

The Supporting Information is available free of charge on the ACS Publications website at DOI: 10.1021/acs.jpca.6b12770.

IR spectra; relative populations, stabilizations energies, and incremental association energies; ETH and MFE clusters; topological parameters, electron densities, Laplacians, kinetic energies, potential energies, and total energies; anharmonic vibration frequencies (PDF)

■ AUTHOR INFORMATION

Corresponding Author

*P. C. Singh. E-mail: sppcs@iacs.res.in.

ORCID

Biswajit Biswas: 0000-0002-9075-1689

Prashant Chandra Singh: 0000-0001-9357-9039

Notes

The authors declare no competing financial interest.

■ ACKNOWLEDGMENTS

This work is supported partially by the research grants provided by the Council of Scientific and Industrial Research (CSIR) [Grant No. 01(2803)/14/EMR-II] as well as Department of Science and Technology (DST-SERB) [Grant No. EMR/2015/001605] India. B.B. thanks CSIR for the fellowship. The authors also thank to Dr. Biman Jana for help in MD simulations and Abha Bhattacharya for critical reading of the manuscript.

■ REFERENCES

(1) Buer, B. C.; Salud-Bea, R.; Al Hashimi, H. M.; Marsh, E. N. G. Engineering Protein Stability and Specificity Using Fluorous Amino Acids: The Importance of Packing Effects. *Biochemistry* **2009**, *48*, 10810−10817.

(2) Marsh, E. N. G. Fluorinated Proteins: From Design and Synthesis to Structure and Stability. *Acc. Chem. Res.* **2014**, *47*, 2878−2886.

(3) Deng, W.-Q.; Molinero, V.; Goddard, W. A. Fluorinated Imidazoles as Proton Carriers for Water-Free Fuel Cell Membranes. *J. Am. Chem. Soc.* **2004**, *126* (48), 15644−15645.

(4) Zhou, P.; Zou, J.; Tian, F.; Shang, Z. Fluorine Bonding−How Does It Work In Protein−Ligand Interactions? *J. Chem. Inf. Model.* **2009**, *49*, 2344−2355.

(5) Gast, K.; Zirwer, D.; Müller-Frohne, M.; Damaschun, G. Trifluoroethanol-Induced Conformational Transitions of Proteins: Insights Gained from the Differences Between α-Lactalbumin and Ribonuclease A. *Protein Sci.* **1999**, *8*, 625−634.

(6) Gerig, J. T. Toward A Molecular Dynamics Force Field for Simulations of 40% Trifluoroethanol−Water. *J. Phys. Chem. B* **2014**, *118*, 1471−1480.

(7) Guo, M.; Mei, Y. Equilibrium and Folding Simulations of NS4BH2 in Pure Water and Water/2,2,2-Trifluoroethanol Mixed Solvent: Examination of Solvation Models. *J. Mol. Model.* **2013**, *19*, 3931−3939.

(8) Jalili, S.; Amani, P. Molecular Dynamics Simulation Study of Solvation Effects of Water and Trifluoroethanol on Gamma-Amino-butyric Acid (GABA). *J. Mol. Liq.* **2014**, *197*, 27−34.

(9) Roccatano, D.; Colombo, G.; Fioroni, M.; Mark, A. E. Mechanism by Which 2,2,2-Trifluoroethanol/Water Mixtures Stabilize Secondary-Structure Formation in Peptides: A Molecular Dynamics Study. *Proc. Natl. Acad. Sci. U. S. A.* **2002**, *99*, 12179−12184.

(10) Mondal, S.; Halder, R.; Biswas, B.; Jana, B.; Singh, P. C. Solvent Organization Around the Perfluoro Group of Coumarin 153 Governs its Photophysical Properties: An Experimental and Simulation Study of Coumarin Dyes in Ethanol as well as Fluorinated Ethanol solvents. *J. Chem. Phys.* **2016**, *144*, 184504.

(11) Evans, M. E.; Burke, C. L.; Yaibuathes, S.; Clot, E.; Eisenstein, O.; Jones, W. D. Energetics of C−H Bond Activation of Fluorinated Aromatic Hydrocarbons Using a [Tp′Rh(CNneopentyl)] Complex. *J. Am. Chem. Soc.* **2009**, *131*, 13464−13473.

(12) Clot, E.; Eisenstein, O.; Jasim, N.; Macgregor, S. A.; McGrady, J. E.; Perutz, R. N. C−F and C−H Bond Activation of Fluorobenzenes and Fluoropyridines at Transition Metal Centers: How Fluorine Tips the Scales. *Acc. Chem. Res.* **2011**, *44*, 333−348.

(13) Yu, Y.; Lin, K.; Zhou, X.; Wang, H.; Liu, S.; Ma, X. New C−H Stretching Vibrational Spectral Features in the Raman Spectra of Gaseous and Liquid Ethanol. *J. Phys. Chem. C* **2007**, *111*, 8971−8978.

(14) Vrhovšek, A.; Gereben, O.; Jamnik, A.; Pusztai, L. Hydrogen Bonding and Molecular Aggregates in Liquid Methanol, Ethanol, and 1-Propanol. *J. Phys. Chem. B* **2011**, *115*, 13473−13488.

(15) Takamuku, T.; Saisho, K.; Nozawa, S.; Yamaguchi, T. X-ray Diffraction Studies on Methanol−Water, Ethanol−Water, and 2-Propanol−Water Mixtures at Low Temperatures. *J. Mol. Liq.* **2005**, *119*, 133−146.

(16) Singh, P. P.; Sharma, B. R.; Sidhu, K. S. Thermodynamics of Chloroform and Methanol Mixtures. *Can. J. Chem.* **1979**, *57*, 387−393.

(17) Silva, P. L.; Bastos, E. L.; El Seoud, O. A. Solvation in Binary Mixtures of Water and Polar Aprotic Solvents: Theoretical Calculations of the Concentrations of Solvent−Water Hydrogen-Bonded Species and Application to Thermosolvatochromism of Polarity Probes. *J. Phys. Chem. B* **2007**, *111*, 6173−6180.

(18) Scott, T. A. Refractive Index of Ethanol−Water Mixtures and Density and Refractive Index of Ethanol−Water−Ethyl Ether Mixtures. *J. Phys. Chem.* **1946**, *50*, 406−412.

(19) Saiz, L.; Padró, J. A.; Guàrdia, E. Structure and Dynamics of Liquid Ethanol. *J. Phys. Chem. B* **1997**, *101*, 78−86.

(20) Plyler, E. K. Infrared Spectra of Methanol, Ethanol, and n-Propanol. *J. Res. Natl. Bur. Stand.* **1952**, *48*, 281−286.

(21) George, W. O.; Has, T.; Fokhray Hossain, M.; Jones, B. F.; Lewis, R. Hydrogen-Bonded Forms of Ethanol-IR Spectra and Ab-initio Computations. *J. Chem. Soc., Faraday Trans.* **1998**, *94*, 2701−2708.

(22) Mejia, S. M.; Mills, M. J. L.; Shaik, M. S.; Mondragon, F.; Popelier, P. L. A. The Dynamic Behavior of a Liquid Ethanol-Water Mixture: A Perspective from Quantum Chemical Topology. *Phys. Chem. Chem. Phys.* **2011**, *13*, 7821−7833.

(23) Ghoufi, A.; Artzner, F.; Malfreyt, P. Physical Properties and Hydrogen-Bonding Network of Water−Ethanol Mixtures from Molecular Dynamics Simulations. *J. Phys. Chem. B* **2016**, *120*, 793−802.

(24) Gereben, O.; Pusztai, L. Investigation of the Structure of Ethanol−Water Mixtures by Molecular Dynamics Simulation I: Analyses Concerning the Hydrogen-Bonded Pairs. *J. Phys. Chem. B* **2015**, *119*, 3070−3084.

(25) Gereben, O. Ring Structure Analysis of Ethanol−Water mixtures. *J. Mol. Liq.* **2015**, *211*, 812−820.

(26) Hagen, K.; Hedberg, K. Conformational analysis. III. Molecular Structure and Composition of 2-Fluoroethanol as Determined by Electron Diffraction. *J. Am. Chem. Soc.* **1973**, *95*, 8263−8266.

(27) Cormanich, R. A.; Rittner, R.; Freitas, M. P.; Bühl, M. The seeming lack of CF···HO Intramolecular Hydrogen Bonds in Linear Aliphatic Fluoroalcohols in Solution. *Phys. Chem. Chem. Phys.* **2014**, *16*, 19212.

(28) Chitra, R.; Smith, P. E. A Comparison of the Properties of 2,2,2-Trifluoroethanol and 2,2,2-Trifluoroethanol/Water Mixtures Using Different Force Fields. *J. Chem. Phys.* **2001**, *115*, 5521−5530.

(29) Buckley, P.; Giguère, P. A.; Yamamoto, D. Infrared Studies on Rotational Isomerism. II. 2-Fluoroethanol. *Can. J. Chem.* **1968**, *46*, 2917−2923.

(30) Dunitz, J. D.; Taylor, R. Organic Fluorine Hardly Ever Accepts Hydrogen Bonds. *Chem. - Eur. J.* **1997**, *3* (1), 89−98.
(31) Laurence, C.; Graton, J.; Berthelot, M.; Besseau, F. O.; Le Questel, J.-Y.; Luçon, M.; Ouvrard, C.; Planchat, A.; Renault, E. An Enthalpic Scale of Hydrogen-Bond Basicity. 4. Carbon π Bases, Oxygen Bases, and Miscellaneous Second-Row, Third-Row, and Fourth-Row Bases and a Survey of the 4-Fluorophenol Affinity Scale. *J. Org. Chem.* **2010**, *75*, 4105−4123.
(32) Rosenberg, R. E. Does Fluoromethane Form a Hydrogen Bond with Water? *J. Phys. Chem. A* **2012**, *116*, 10842−10849.
(33) Rosenberg, R. E. Microsolvation of Fluoromethane. *J. Phys. Chem. A* **2016**, *120*, 7519−7528.
(34) Schneider, H.-J. Hydrogen Bonds with Fluorine. Studies in Solution, in Gas phase and by Computations, Conflicting Conclusions from Crystallographic Analyses. *Chemical Science* **2012**, *3*, 1381−1394.
(35) Frisch, M. J.; Trucks, G. W. T; Schlegel, H. B.; Scuseria, G. E.; Robb, M. A.; Cheeseman, J. R., Scalmani, G.; Barone, V.; Mennucci, B.; Petersson, G. A.; et al. *Gaussian 09*, revision B.01; Gaussian, Inc.: Wallingford, CT, 2010.
(36) Bader, R. F. W. *Atoms in Molecules- A Quantum Theory*; Oxford University Press: New York, 1990.
(37) Spoel, D. V.; Hess, E. L.; Van Buuren, A. R.; Apol, E.; Meulenhoff, P. J.; Tieleman, D. P.; Sijbers, A. L.; Feenstra, K. A.; Van Drunen, R.; Berendsen, H. J. *Gromacs User Manual*, www.gromacs.org, 2014.
(38) Canzar, S.; El-Kebir, M.; Pool, R.; Elbassioni, K.; Malde, A. K.; Mark, A. E.; Geerke, D. P.; Stougie, L.; Klau, G. W. Charge Group Partitioning in Biomolecular Simulation. *J. Comput. Biol.* **2013**, *20*, 188−198.
(39) Berendsen, H. J. C.; Postma, J. P. M.; Van Gunsteren, W. F.; Dinola, A.; Haak, J. R. Molecular Dynamics with Coupling to An External Bath. *J. Chem. Phys.* **1984**, *81*, 3684−3690.
(40) Parrinello, M.; Rahman, A. Polymorphic Transitions in Single Crystals: A New Molecular Dynamics Method. *J. Appl. Phys.* **1981**, *52*, 7182−7190.
(41) Mondal, S.; Teja, A. U.; Singh, P. C. Theoretical Study on the Microhydration of Atmospherically Important Carbonyl Sulfide in its Neutral and Anionic forms: Bridging the Gap Between the Bulk and Finite Size Microhydrated Cluster. *J. Phys. Chem. A* **2015**, *119*, 3644−52.
(42) Mondal, S.; Teja, A. U.; Singh, P. C. Effect of Microhydration on the Atmospherically Important Metastable Carbonyl Sulfide Anion: Structure, energetic, and infrared study. *Int. J. Quantum Chem.* **2015**, *115*, 785−795.
(43) Mondal, S.; Chandra Singh, P. Noble Gas Induced Surprisingly Higher Stability of π Hydrogen Bonded Complex: Comparative Study of Hydrogen Bonded Complexes of HKrCCH and HCCH with H_2O, NH_3, CH_3OH and CH_3NH_2. *RSC Adv.* **2014**, *4*, 20752−20760.
(44) Biswas, B.; Singh, P. C. Effect of Hydration on the Organo-Noble Gas Molecule HKrCCH: Role of Krypton in the Stabilization of Hydrated HKrCCH complexes. *Phys. Chem. Chem. Phys.* **2015**, *17*, 30632−41.
(45) Heger, M.; Scharge, T.; Suhm, M. A. From Hydrogen Bond Donor to Acceptor: The Effect of Ethanol Fluorination on the First Solvating Water Molecule. *Phys. Chem. Chem. Phys.* **2013**, *15*, 16065−16073.
(46) Dixit, S.; Crain, J.; Poon, W. C. K.; Finney, J. L.; Soper, A. K. Molecular Segregation Observed in a Concentrated Alcohol-Water solution. *Nature* **2002**, *416*, 829−832.
(47) Hobza, P.; Havlas, Z. Blue-Shifting Hydrogen Bonds. *Chem. Rev.* **2000**, *100* (11), 4253−4264.
(48) Thakur, T. S.; Kirchner, M. T.; Blaser, D.; Boese, R. Nature and Strength of C-H···O Interactions Involving Formyl Hydrogen Atoms: Computational and Experimental Studies of Small Aldehydes. *Phys. Chem. Chem. Phys.* **2011**, *13* (31), 14076−14091.

DOI: 10.1021/acs.jpca.6b12770
J. Phys. Chem. A 2017, 121, 1250−1260